Hydrogen separation performance of CMS membranes derived from the imide-functional group of two similar types of precursors

Arun Kumar Itta [a], Hui-Hsin Tseng [b,c,*]

[a] Department of Environmental Engineering, National Chung Hsing University, Taichung 402, Taiwan, ROC
[b] School of Occupational Safety and Health, Chung Shan Medical University, Taichung 402, Taiwan, ROC
[c] Department of Occupational Medicine, Chung Shan Medical University Hospital, Taichung 402, Taiwan, ROC

ARTICLE INFO

ABSTRACT

Carbon molecular sieve (CMS) membranes derived from polyimide (PI) and polyetherimide (PEI), which have similar functional groups were fabricated for gas separation. To evaluate the effect of the functional groups of PI and PEI on the properties of their CMS membranes, the composition of the casting solution and carbonization temperatures were investigated. Thermogravimetric analysis (TGA), fourier transform infrared spectroscopy (FTIR) and field emission scanning electron microscopy (FE-SEM) were employed to characterize thermal stability, functional groups and microstructural change in the derived CMS membrane. The gas permeation performance of the CMS membranes were estimated using four gases: hydrogen, carbon dioxide, nitrogen and methane. The results show that C=C stretching in imides exhibit an intense absorption peak at 1665 cm^{-1} with PI dominating the insignificant degradation of the imide groups at the intermediate stage. For PEI, the absorption peaks of C–N stretching and C–C–C bending were intense at 1011 and 1068 cm^{-1} respectively, dominating the ethers and cyclic ethers of asymmetric stretching. The microstructure and gas permeation properties of the obtained CMS membranes were significantly affected by the functional group of precursors and their concentrations in the casting solution. Optimized performance for hydrogen permeation (565 Barrer) [1 Barrer = 1×10^{-10} cm^3 (STP) cm/(cm^2 s cmHg)] was obtained with PI-10-600 CMS membrane. The best selectivity for H_2/N_2 at 33.2 was obtained from PI-10-500 CMS membrane.

1. Introduction

Hydrogen has recently attracted significant interest because of its potential to become a renewable energy carrier based on its possible applications, such as energy recovering systems involving various general fuels, fuel cells and storage carriers. Membrane-related processes are considered to be one of the most promising technologies in producing [1,2] and purifying [3,4] high-purity hydrogen, because of lower energy consumption, lower capital, lower maintenance cost, and higher production efficiency. Comparing with other separation processes, membrane technology for hydrogen separation are more suitable for various area applications [5,6]. Polymeric membrane materials are widely used for the

hydrogen purification and its future prospective and contemporary approaches [7]. However, there are some draw backs in these polymeric membranes such as aging [8] and plasticization [9], therefore the separation performances were suffered [10]. These draw backs have led to further trails to develop or identify the new type of materials, hence inorganic materials were identified and it can be used as superior membrane material for hydrogen purification compared to polymeric membranes [11—14], such as silica- and alumina-based inorganic membrane, zeolite, palladium- based membrane [1,6], and molecular sieve carbon-based membrane. Among them, carbon molecular sieve (CMS) membrane has attracted much attention due to its high gas permeability and selectivity, as well as its excellent chemical and thermal stability [15]. The concept of separation perfor- mance in CMS membranes is dependent on the pore size, which determines the degree of interaction between mole- cules and pores. As per the new environmental regulations, hydrogen recovery from refinery streams in petrochemical industry increased the demand for hydrotreating, hydro- cracking or hydrodesulfurization processes [16]. Recent CMS membrane studies confirm that the hydrogen from light hydrocarbons such as methane is better choice materials for hydrogen permeability and selectivity [17]. CMS membranes also show superior permeability and selectivity factors compared with polymeric membranes in the presence of organic vapor and non oxidizing acids and bases environ- ment [10]. However, in gas separation applications, a trade- off relationship generally exists between permeability and permselectivity, in which improved permeability is generally accomplished with decreased permselectivity and vice versa [18,19]. The key research interest is to develop CMS membranes with high permeability and high permselectivity.

Generally, CMS membrane is pyrolyzed from the polymer membrane, in which the (1) chemical structure of the polymer precursor [20,21], (2) pre-treatment [22—26], (3) pyrolysis conditions [27,28], and (4) surface modifications [29—31] were considered important factors influencing the final properties of the CMS membrane. Previous investigations [27,28] paid much attention on the effect of pyrolysis conditions such as pyrolysis temperature, carbonization environment, heating rate and soaking time on the microstructure of the final CMS membrane and gas separation performance. These results indicate that as pyrolysis temperature increases, the thermal-less side group of the polymer would be removed and result in a porous structure. Further, as the temperature increases and reaches the carb- onized temperature, the steric structure would collapse and result in a dense carbon matrix. Therefore, proper pyrolysis conditions should exist for all polymer precursors. However, although considering pyrolysis protocols as a key factor to control the microstructure of the CMS membrane, the problem of trade-off relationship between permeability and permse- lectivity still cannot be solved due to its intrinsic quality.

Some research groups studied CMS membrane perfor- mance related to the structural characteristics of the polymer precursor [20,21,32,33]. Jung et al. [20] introduced five commercial polymers to prepare carbon membranes and indicated two distinctive trends in terms of their gas perme- ation characteristics. Carbon membranes derived from PI, PEI and phenolic resin showed typical molecular sieving mechanisms for all gases. However, gas permeation through the polyacrylonitrile and cellulose acetate-derived carbon membrane exhibited intermediate behavior between Knud- sen diffusion and molecular sieving due to the large pore size distribution in the carbon matrix. These results prove that the chemical structure of the polymer precursor (not pyrolysis conditions) is the dominant factor in preparing molecular sieving carbon membrane. Kim et al. [32] investigated the effect of side groups on improving the gas separation perfor- mance of CMS membranes. The authors synthesized poly- imides (PIs) with a varying number of carboxylic acid groups and pyrolyzed at high temperature to fabricate CMS membrane. The results indicated that removing the carbox- ylic acid pendent side groups resulted in a large pore volume in the carbon matrix and improved gas permeabilities with increasing carboxylic acid group content. Song et al. [21] synthesized two kinds of poly (furfuryl alcohol) (PFA) composed of a large amount of same-functional groups by a different cross-linking style. After pyrolysis, the results indicated that the furan ring linked to the aromatic chain exhibited more thermal stability and smaller interlayer spacing than that linked to linear alkyl, which is related to low gas permeability and high permselectivity. The effects of polymeric precursor structure on the gas separation perfor- mance are summaries in Table 1.

PI has high intrinsic gas permeability as well as high selec- tivity compared with other polymeric precursors. Generally, PI can be synthesized with various dianhydrides and diamines to obtain desirable gas separation properties and its separation performance relies on its chemical structure. Compared with PI, polyetherimide (PEI) not only possesses imide units that provide stiffness and heat resistance, but also has flexible ether linkages, which provide good process ability [34,35]. Thus, comparing PEI with PI to fabricate CMS membranes may show significant differences in microstructure and gas separation performance for the resultant CMS membranes. To investigate the effect of functional groups on the microstructure of the carbon matrix, the polymer concentration of the casting solu- tion and the pyrolysis condition are thoroughly examined.
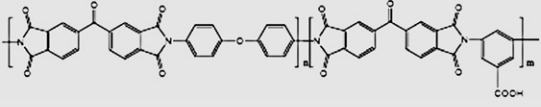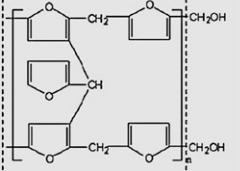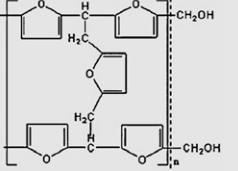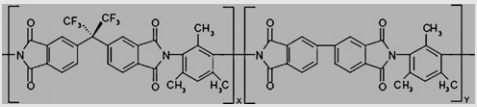
2. Experimental method
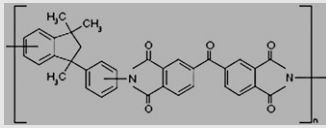
2.1. Materials

The pure polymer precursors PI resin and PEI were purchased from Alfa Aesar and Aldrich Co., USA. The chemical structures and the characteristics of these two polymers are shown in Table 2. N-methyl-2-pyrolidone (NMP) solvent was purchased from Mallinckrodt Chemicals Company, USA, and was used without further purification. The alumina disks with average pore size of 0.14 μm, diameter of 23 mm and porosity of 40—48% was purchased from Ganya Fine Ceramics Co., Taiwan and was used as membrane support.

2.2. Fabrication of CMS membranes

The synthesis of PI- and PEI-derived CMS membranes was conducted via a two-step procedure. First, Al_2O_3 supported polymeric dense films were fabricated by spin coating

Table 1 – Effect of polymeric precursor structure on the gas separation performance.

Polymer	Chemical structure	Pyrolysis condition	Gas separation performance	Ref.
Polyimide with carboxylic acid groups		700 °C Ar gas	P_{O_2} = 707 Barrer S_{O_2/N_2} = 9	[32]
Poly(furfuryl alcohol) (PFA)	Type I Type II	600–900 °C Ar gas	P_{O_2} = 6/mol m^{-2} s^{-1} Pa^{-1} × 10^{-10} S_{O_2/N_2} = 9	[21]
6FDA/BPDA-DAM	The ration of X to Y is 1:1.	550 °C 1ppm O_2/Ar gas	P_{O_2} = 1530 Barrer S_{O_2/N_2} = 7.5	[33]
BTDA-DAPI (Matrimid)		550 °C 1ppm O_2/Ar gas	P_{O_2} = 301 Barrer SO_2/N_2 = 4.8	[33]

1 Barrer = 1 × 10^{-10} cm^3 (STP) cm/(cm^2 s cmHg).

method. The composition of PI and PEI casting solutions are presented in Table 3. PI or PEI was dissolved in NMP solvent using a magnetic stirrer for 24 h at 60–80 °C to prepare homogeneous coating solution. PI or PEI solution was followed by coating on the surface of Al_2O_3 support by spin coating technique with 2000 rpm for 15 s. Then, the polymer films were formed after drying at room temperature for 24 h. Subsequently, the polymer films were pyrolyzed on a heating furnace with a quartz tube (as shown in Fig. 1) at temperature ranged from room temperature to 500–600 °C. They were cured at a heating rate of 5 °C min^{-1} from room temperature to 240 °C under a vacuum system and kept at 240 °C for 6 h to remove the excess solvent. Then, the pyrolysis temperature was programmed from 240 °C to 500 °C and 600 °C respectively, at a heating rate of 5 °C min^{-1} and held at the final temperature for 1 h. The membrane code was denoted as PI (or PEI)-X-Y where X is the polymer concentration and Y is the pyrolysis temperature. For example, PEI-10-500 means the PEI-10-derived CMS membrane pyrolyzed at 500 °C.

2.3. Gas permeation measurements

A standard vacuum time-lag method was used to measure the single-gas permeabilities at 25 °C. Feed pressure of 2 atm on H_2 (0.289 nm), CO_2 (0.33 nm), N_2 (0.364 nm) and CH_4 (0.38 nm) were tested in this study. The experimental setup has been illustrated in our previous study [36]. Leak detection tests were performed
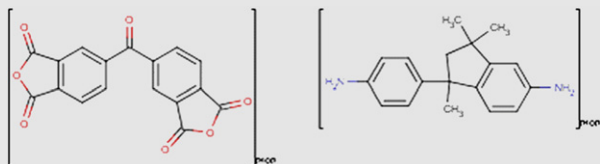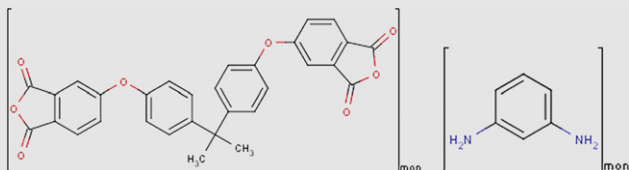
in all valves prior to the experiments. Additionally, each time the membrane was changed, it was exposed overnight to vacuum prior to measurement until both the feed and permeate sides of the membrane cell were evacuated to lower than 10^{-5} Torr. The pressure was measured using pressure transducers and the data were recorded using the VisiDaq Builder software.

The permeability coefficients were determined by the following equation:

$$P = \frac{dp}{dt}\left(\frac{V \cdot T_0 \cdot L}{p_0 \cdot T \cdot \Delta p \cdot A}\right)$$

where P is the permeability expressed in Barrer [1 Barrer = 1 × 10^{-10} cm^3 (STP) cm/(cm^2 s cmHg)], dp/dt the rate of pressure rise at the steady state, V (cm^3) the calibrated downstream volume, L (cm) the membrane thickness, Δp (cmHg) the pressure difference between the feed side and the permeate side, T (K) the measurement temperature, A (cm^2) the effective area of the membrane, and p_0 and T_0 the standard pressure and temperature, respectively. Permselectivity was defined in this study as the ideal separation factor, which is expressed by $\alpha_{A/B} = P_A/P_B$, where P_A and P_B are the permeability coefficients for gas A and B, respectively. Six samples were prepared based on each condition and subjected to the independent permeation test. The permeation values were the average (with the standard deviation) of at least three independent measurements.

Table 2 – Chemical structures and characteristics of PI and PEI used in this study.

Polymer	Molecular structure/Synonyms	T_{decom} (°C)
PI	1,3-isobenzofurandione, 5, 5′-carbonylbis-, polymer with 1 (or 3)-4-4aminophenyl-2, 3-dihydro-1,3,3 (or 1,1,3)-trimethyl-1H-inden-5-amine	520.12
PEI	Poly(Bisphenol A-co-4-nitrophthalic anhydride-co-1,3-phenylenediamine); 5,5′-[propane-2,2-diylbis(benzene-4,1-diyloxy)]=bis(2-benzofuran-1,3-dione)-benzene-1,3-diamine (1:1)	514.45

2.4. Characterization of CMS membranes

The thermal decomposition of the polymer precursor during pyrolysis was characterized by thermogravimetric analysis (TGA) using a TGA Seiko SSC 5000 thermogravimetric analyzer. The analysis was carried out with a ramp of 10 °C min^{-1} at a temperature range of 50–700 °C. The flow rate of pure nitrogen gas was controlled at 50 ml min^{-1}. Fourier transform infrared spectrometry (FTIR) of PI- and PEI-based polymeric membranes and pyrolysis at different temperatures of carbon membranes were recorded using JASCO-4100 FTIR spectrophotometer in an attenuated total reflection mode (FTIR-ATR). Finally, the surface morphologies of the prepared CMS membranes were investigated using a field emission scanning electron microscopy (FE-SEM) JSM 5600 device.

3. Results and discussion

3.1. Characterization of CMS membranes

3.1.1. TGA
Since CMS membranes are typically derived from pyrolyzed polymeric membranes, the thermal decomposition behavior of pure polymers and their derived polymeric membranes

Table 3 – Composition of casting solution for fabricating CMS membrane in this study.

Sample code	Composition of casting solution (wt.%)		
	PI	PEI	NMP
PI-5	5	0	95
PI-10	10	0	90
PEI-5	0	5	95
PEI-10	0	10	90

were first investigated to evaluate the structural properties of the polymer. Fig. 2 illustrates the TG curves obtained at room temperature up to 700 °C under nitrogen flow. The TG analysis showed that pure polymer PI [Fig. 2(a)] and PEI [Fig. 2(b)] exhibited no distinct weight loss below 450 °C. PI and PEI showed weight loss from 500 to 600 °C, and finally about 65% of the weight residue was remained at 700 °C. However, from 500 to 600 °C the thermal decomposition rate of PEI is higher than that of PI. This can be explained by different thermal degradation routes between PI and PEI. Generally, the thermal decomposition of organic polymers is characterized by the breakage of the main chains [37]. Among these two polymer precursors, PI has more aromatic or cyclic groups which is responsible for it's the higher thermal stability.

For polymeric membranes PI-5, PI-10, PEI-5 and PEI-10, the TG curves indicated two distinctive trends in terms of thermal decomposition rate. Polymeric membranes derived from PI, however, showed [Fig. 2(c)] higher weight loss before 500 °C. The weight loss of PI-5 began early at approximately 200 °C due to the early loss of the solvent in the membrane because of the low weight loading of the polymer concentration. The early loss was followed by a final decomposition that began slowly at approximately 500 °C Fig. 2(d) illustrates the early weight loss of PI-10 that began at approximately 250 °C. Subsequently, final decomposition began slowly at approximately 520 °C.

Fig. 2(e and f) of PEI-5 and PEI-10, respectively, showed initial weight losses around 230 °C, followed by a final decomposition that began slowly at around 530 °C. This may be due to the evolution of CO, CO_2 and CH_4 that may have caused a cleavage in the benzene ring of the PEI precursor. The maximum weight loss rates were noted at a temperature range of 550–600 °C.

Fig. 2 also shows that PI-based membranes had a slightly smaller weight residue on the pyrolysis samples compared with the PEI-based membranes at 500 °C. This may be due to the quick evaporation of the solvent in the early stages that may result in the forming uniform pores on the final carbon film. As shown in Fig. 5, the low thermal resistance (based on weight
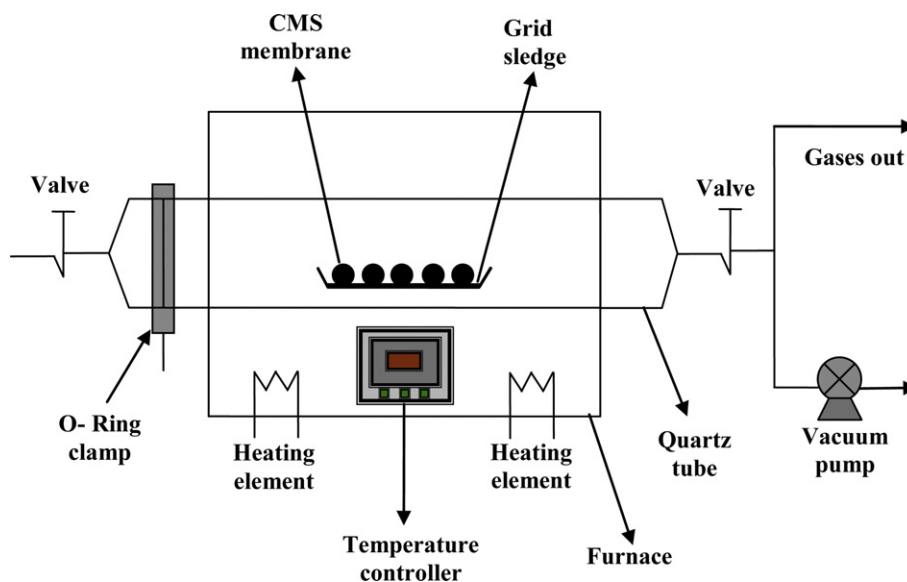
Fig. 1 — Schematic representation of pyrolysis setup.

residue) of PI-based membranes raised the possibility of forming big pores on the membrane morphology compared with PEI-based membranes (see Section 3.1.3.). However, in the final decomposition, PEI-based membranes had slightly higher weight loss than PI-based membranes, which may be attributed to the breakage of ether groups in the polymer chain.

3.1.2. FTIR analysis

Fig. 3 shows the typical FTIR spectra of pure PI-10 polymer and PI-10-based carbon membranes with different pyrolysis temperatures. As shown in Fig. 3(a), PI-10 polymer membrane displays characteristic peaks located at 1097, 1162, 1249, 1370, 1485, 1509, 1665, 1713 and 1779 cm^{-1} which are assigned to the C–C–C bending, C–O stretching, C–H stretching, CH_3 bending [sym (umbrella)], C=C aromatic ring (stretching), C=C stretching, C=O symmetrical stretching, and C=O asymmetrical stretching, respectively. This conforms to the FTIR spectra analysis of PI conducted by other groups [38–40]. As the PI-10 polymer membrane pyrolyzed at different temperatures, the intensity of characteristic peaks decreased as the temperature increased. These results revealed that the functional groups of

PI reduction with the increase of pyrolysis temperature due to the thermal decomposition. The changes of infrared absorption spectra were summarized in Table 4. Minimal visible changes were observed for the FTIR-(ATR) spectra of membranes pyrolyzed at 300–400 °C, and small weight loss degradation was also observed from the TGA analysis during this temperature range (Fig. 2). At approximately 400–450 °C, the polymer began to transform from an amorphous into an intermediate state, in which the polymer expanded thermally with a slight decrease in weight and absorption peak intensity (Table 4 and Fig. 2). As indicated by the TGA and FTIR data (Fig. 2 and Table 4), notable changes in chemical composition were encountered at a temperature range of approximately 450–500 °C, in which increments in the polymer chain mobility accompanied by high degradation rates was detected. At 500–550 °C, the polymer underwent maximum decomposition rate and significant physicochemical development crucial for carbon structure and pore formation. The degradation of
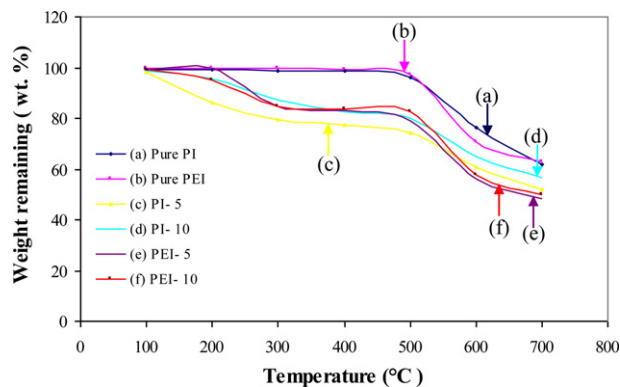

Fig. 2 — TGA curves for the pure polymers (a) PI, (b) PEI and polymeric membranes (c) PI-5, (d) PI-10, (e) PEI-5, and (f) PEI-10.
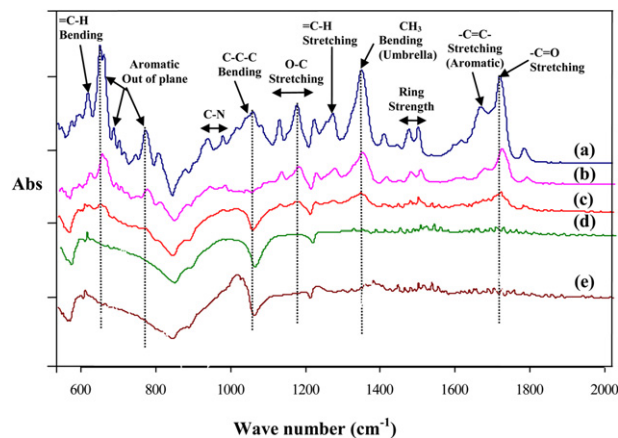

Fig. 3 — FTIR spectra of (a) PI-10 polymeric membrane and (b) PI-10-300, (c) PI-10-400, (d) PI-10-500, and (e) PI-10-600 carbon membranes.
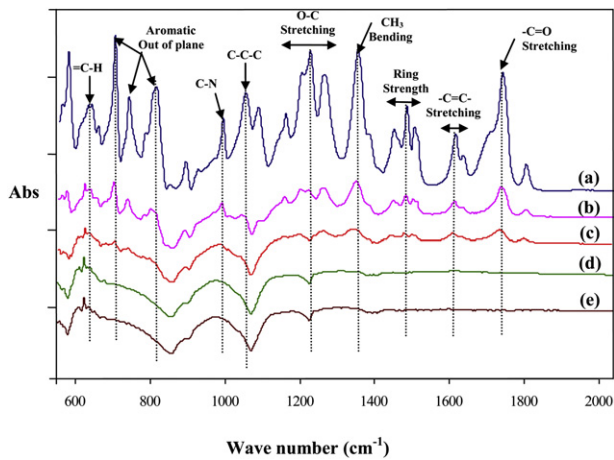
Fig. 4 – FTIR spectra of (a) PEI-10 polymeric membrane and (b) PEI-10-300, (c) PEI-10-400, (d) PEI-10-500, and (e) PEI-10-600 carbon membranes.

polymer was governed by the transformation of imide groups [41]. This was confirmed by the decline in the intensity of the imide group during heat treatment at 450–500 °C, as shown in Table 4 and Fig. 2.

Fig. 4a displays the FTIR-ATR spectra of PEI-10 polymer membrane. Compared with PI-10 membrane, the new appearances of the bands at 1011 and 1068 cm^{-1} were observed, which results from the stretching vibration of C–N and C–C–C. These are due to the presence of ethers and cyclic ethers of

asymmetric stretching. Peaks at approximately 1101 cm^{-1}, 1269 and 1352 cm^{-1} indicating the C–C–C bending, C–O stretching and CH$_3$ bending (anti-sym) were also observed. Another peak at approximately 1494 cm^{-1} indicating C=C stretching due to the aromatic functional group was also noted. Peaks at approximately 1777 cm^{-1}, indicating C=O typical of imide carbonyl asymmetric stretching; at 1718 cm^{-1}, corresponding to the C=O symmetric stretching of the imide group; and at 1352 cm^{-1}, corresponding to the CH$_3$ bending of imide group, were further observed [42]. Fig. 4(b)–(e) represents the PEI-based carbon membranes pyrolyzed at 300–600 °C, in which visible changes can be observed (Table 4).

The absorption peaks of PEI-based polymer membranes exhibited similar behaviors with those of PI-based carbon membranes. Strong intensity peaks were observed on PEI-based membranes comparable with those of PI-based membranes. Peaks may have been caused by the light variation in the weight loss of PEI (Fig. 2) on the performance of the CMS membranes. PEI-based membranes show the origin of –C–H and out-of-plane strong intensity peaks comparable with PI-based membranes. These strong intensity peaks were due to ether asymmetric stretching at the peaks.

3.1.3. FE-SEM

The FE-SEM microphotographs of PI- and PEI-derived CMS membranes were shown in Fig. 5. As shown in Fig. 5a, the PI-5-500 carbon layer with a dense film structure was formed on the surface of the macroporous alumina support. The thickness of the PI-5-500 carbon layer was measured to about 4 μm. Fig. 5b shows the surface view of the PI-5-500 CMS

Table 4 – Infrared absorption bands of PI- and PEI-based polymeric membrane and carbon membranes.

Origin	Absorption bands (cm^{-1})										Intensity
	PI-10 membrane					PEI-10 membrane					
	Polymer-based	Carbon-based with different pyrolyzed temperature (°C)				Polymer-based	Carbon-based with different pyrolyzed temperature (°C)				
		300	400	500	600		300	400	500	600	
=C–H bending	709	709	705	–	–	742	742	742	742	–	vs
–C–H– aromatic	–	–	–	–	–	778	778	778	–	–	
–C–H– out -of- plane	821	821	–	–	–	845	845	–	–	–	s
C–N stretching	980	980	–	–	–	921	920	921	920	–	
C–N stretching	–	–	–	–	–	1011	1011	1011	–	–	s
C–C–C bending	1097	1073	–	–	–	1068	–	–	–	–	s
C–C–C bending	–	–	–	–	–	1101	1101	–	–	–	s
C–O stretching	1162	1159	1158	–	–	1171	1170	–	–	–	s
C–O stretching	1204	1204	1201	–	–	1235	1211	–	–	–	s
=C–H stretching	1249	1249	1247	–	–	–	–	–	–	–	s
C–O stretching	1295	1294	–	–	–	1269	1265	–	–	–	s
CH$_3$ bending; anti-sym and sym (umbrella)	1370	1366	1366	–	–	1352	1350	1350	–	–	vs
CH$_3$ (bending overlap)	1427	1425	–	–	–	1444	–	–	–	–	s
C=C aromatic ring (stretching)	–	–	–	–	–	1477	1475	1475	–	–	s
C=C aromatic ring (stretching)	1485	1485	1490	–	–	1494	1494	1494	–	–	s
C=C aromatic ring (stretching)	1509	1512	1508	–	–	1599	1599	1599	–	–	s
C=C (stretching)	1665	1671	–	–	–	–	–	–	–	–	s
C=O symmetrical stretching	1713	1720	1715	–	–	1718	–	–	–	–	vs
C=O asymmetrical stretching	1779	1777	1775	–	–	1777	1777	–	–	–	w

vs: very strong; s: strong; w: weak.

membrane. The cyclic pores without penetrating from the top to the bottom of the carbon film can be observed. As the pyrolysis temperature increased to 600 °C, the cyclic pores become sponged-like structure (Fig. 5c). These indicate that after pyrolyzed at higher temperature, many thermal-labile functional groups were decomposed and leaved much vacancy on the carbon layer. This phenomenon was consisted with TGA and FTIR results. Similar results were also found in the PI-10-500 (Fig. 5d and e) and PI-10-600 (Fig. 5f) membranes. Although, in the cases of PI-10-derived membranes, fewer pores were observed on the carbon film compared with those in PI-5-derived CMS membranes, the higher pyrolysis temperature also resulted in more porous structure.

Fig. 6a shows the FE-SEM images of the top-view of PEI-5-500, while Fig. 6b shows the top-view of PEI-10-500. No big pores are formed on the carbon film compared with the PI-derived carbon membranes with different concentration and pyrolysis temperature. The top layer is smooth with homogeneous distribution on the carbon matrix of the alumina support. Fig. 6c represents the top-view of PEI-5-600, while Fig. 6d demonstrates the top-view of PEI-10-600. On the surface structure for both pyrolysis temperatures, no big pores were observed compared with the PI-based carbon membranes at different pyrolysis temperatures. This may be because of the nature of the polymer and weight residue at the different pyrolysis temperatures. Fig. 6e represents the cross-sectional
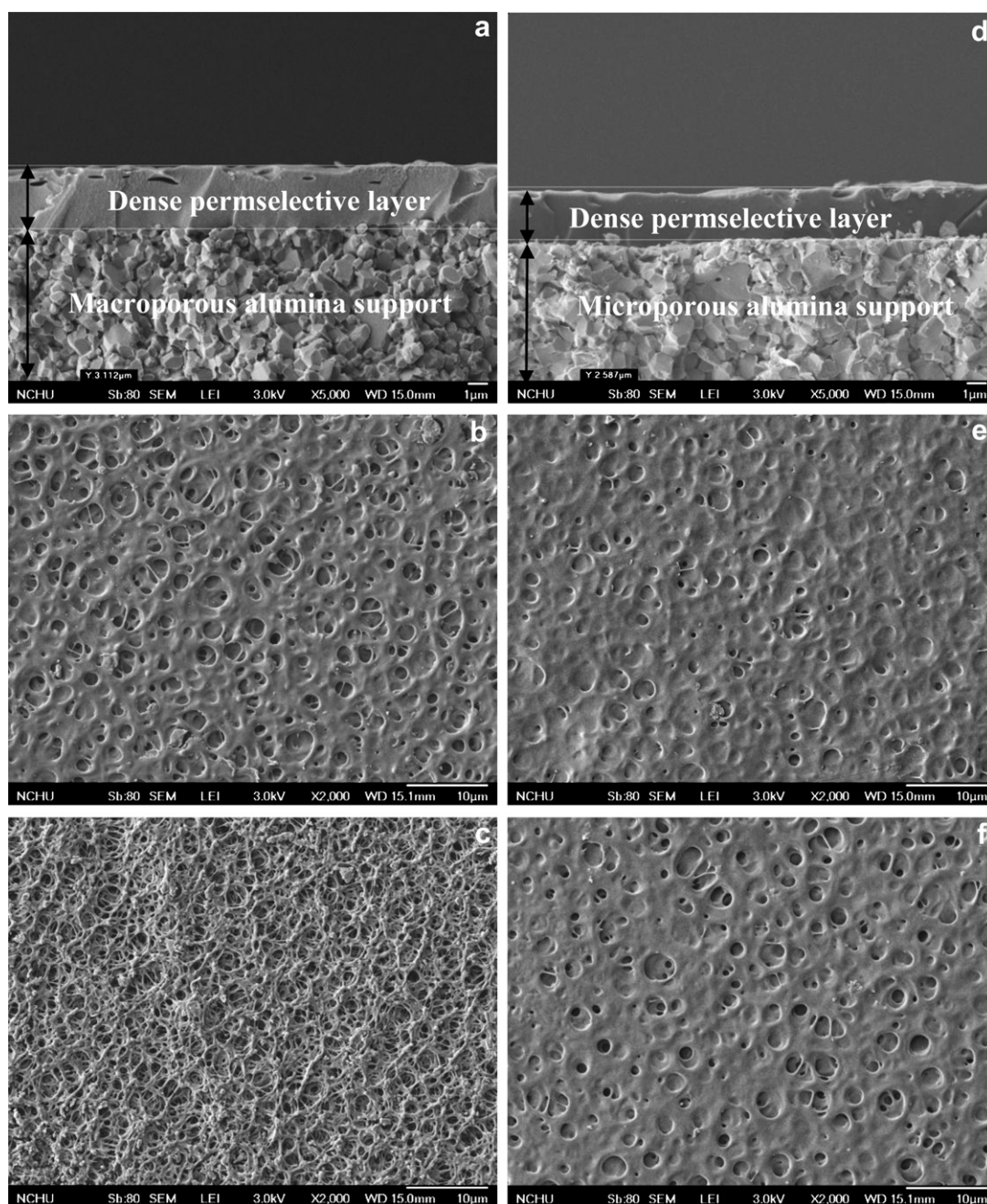

Fig. 5 – **FE-SEM images of PI-derived carbon membranes: (a) cross-section of PI-5-500, (b) top-view of PI-5-500, (c) top-view of PI-5-600, (d) cross-section of PI-10-500, (e) top-view of PI-10-500, (f) top-view of PI-10-600.**

view of PEI-5-500, where the carbon film is a dense permse-lective layer with a thickness of approximately 3−4 μm. Fig. 6f demonstrates the cross-section and top-view of the carbon film at PEI-10-500 membrane. It can be seen that the carbon film shows a very smooth being almost defect-free on the carbon film on the alumina support, which allowed for the achieve-ment of excellent gas permeation rates for the carbon membranes. Compared to the PI-derived CMS membrane, PEI-derived membrane shows a dense film structure, which were not agreed the results obtained from the TGA.

3.2. Gas permeation properties of the PI- and PEI-derived CMS membranes

Gas permeation properties were determined to investigate the molecular sieve capabilities of CMS membranes derived from PI and PEI precursors which possess different functional groups. The results shown in Fig. 7 were obtained by measuring pure gas (i.e. H_2, CO_2, N_2, and CH_4) permeability through the CMS membranes.

3.2.1. PI-derived CMS membranes

For PI-derived CMS membranes (Fig. 7a and b), the H_2 and CO_2 permeabilities increased rapidly with increasing polymeric concentration and pyrolysis temperature from 500 to 600 °C, while the N_2 and CH_4 permeability (Fig. 7c and d) slightly increased. The PI-10-600 shows a higher permeability of 565 Barrer for hydrogen compared with other carbon memb-ranes. Based on the FTIR results (Fig. 2), due to the CH_3 bending, aromatic C=C stretching and C=O symmetrical or asymmetrical stretching effect, the PI structure at early stages of thermal degradation could affect the final permeation rates. It is already confirmed that the transformation of PI polymer was governed by the imide groups [41]. After pyrolyzed at 500
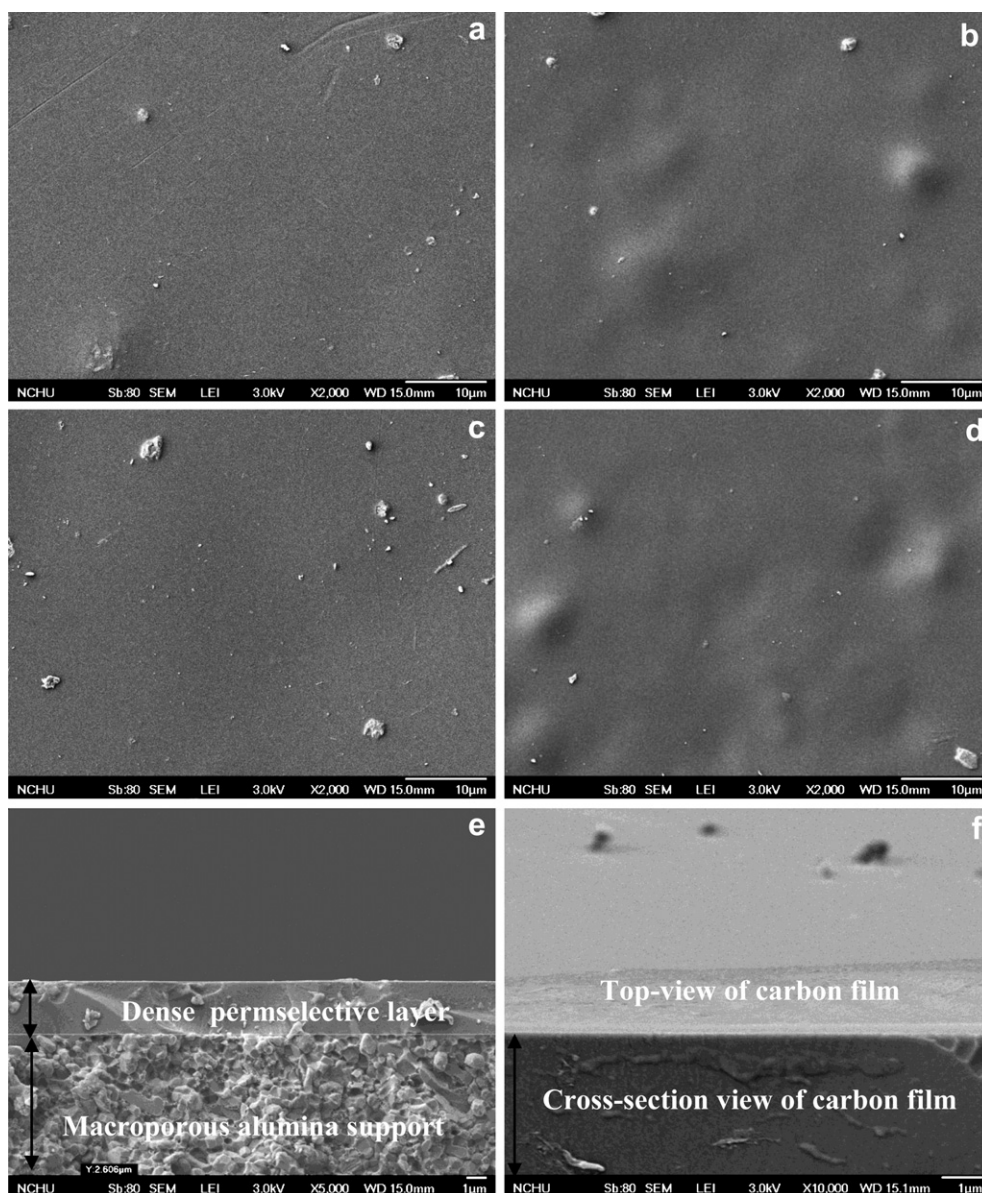

Fig. 6 − **FE-SEM images of PEI-derived carbon membranes: (a) cross-section of PEI-5-500, (b) top-view of PEI-5-500, (c) top-view of PEI-5-600, (d) cross-section of PEI-10-500, (e) top-view of PEI-10-500, (f) top-view of PEI-10-600.**

or 600 °C, the PI polymeric membrane were converted into carbon membrane with porous structure. Generally, the permeabilities of smaller gases through microporous membranes, such as CMS membranes, are concomitant especially with the order of their kinetic diameter of gas molecules through the microporous channels of the CMS membranes [43].

The ideal separation factors illustrated in Fig. 8a—c shows the H_2/CO_2, H_2/N_2, and H_2/CH_4 permselectivities of PI-derived CMS membranes, respectively. The ideal separation factors of PI-5-derived CMS membranes for these three gas pairs were all decreased with the pyrolysis temperature increased from 500 to 600 °C. At pyrolysis temperature range 550—600 °C, weight residue of all the samples gradually decreased as the temperature drastically increased. This may be attributed to the loss of carbon content in the samples at higher temperatures. Generally, for carbon membranes gas molecules permeate through the micropores or sub-micropores of carbon matrix. The average pore sizes were determined by the initial arrangement of polymer chain and the final vacancy leaved in the carbon matrix which caused by thermal-labile functional group decomposition. Based on the TGA and FE-SEM results, it can be found that all the PI-5-derived and PI-10-derived CMS membranes showed more porous structure at higher pyrolysis temperature, which resulted in higher permeability and lower permselectivity. CMS membranes allow considerably high gas permeability through the

micropore channels by molecular sieving mechanism compared to polymer membrane's solution-diffusion mechanism, thus the molecular sieving mechanism plays a key role in gas transport through the micropore channels of the membrane, leading to the enhancement of permselectivities of gas molecules simultaneously [44].

However, in the case of PI-10-derived CSM membranes, the selectivity of H_2/CO_2 slightly increased with the pyrolysis temperature increased to 600 °C. This result indicated that increased PI precursor concentration could increase the residue carbon in the membrane and narrow the pore size close to the dimension of the small kinetic gas molecules, such as H_2, and CO_2, which results in higher permselectivity. Similar results were also found in the H_2/N_2 and H_2/CH_4 gas pair's performance. The PI-10-500 and PI-10-600 CMS membranes showed higher selectivity for H_2/N_2 and H_2/CH_4 than PI-5-derived carbon membranes. Moreover, PI-10-500 membrane facilitated higher carbon membrane separation performance such as permselectivity of H_2/N_2 (=33.2), and H_2/CH_4 (=16.4) than those of other operating conditions of the CMS membranes at 500 °C. This may be due to the higher weight residue at 500 °C compared with that at 600 °C (see Fig. 2).

3.2.2. PEI-derived CMS membranes

Fig. 7 shows the gas permeabilities of PEI-derived CMS membranes obtained from different precursor concentration and pyrolysis temperatures. For PEI-derived CMS membranes
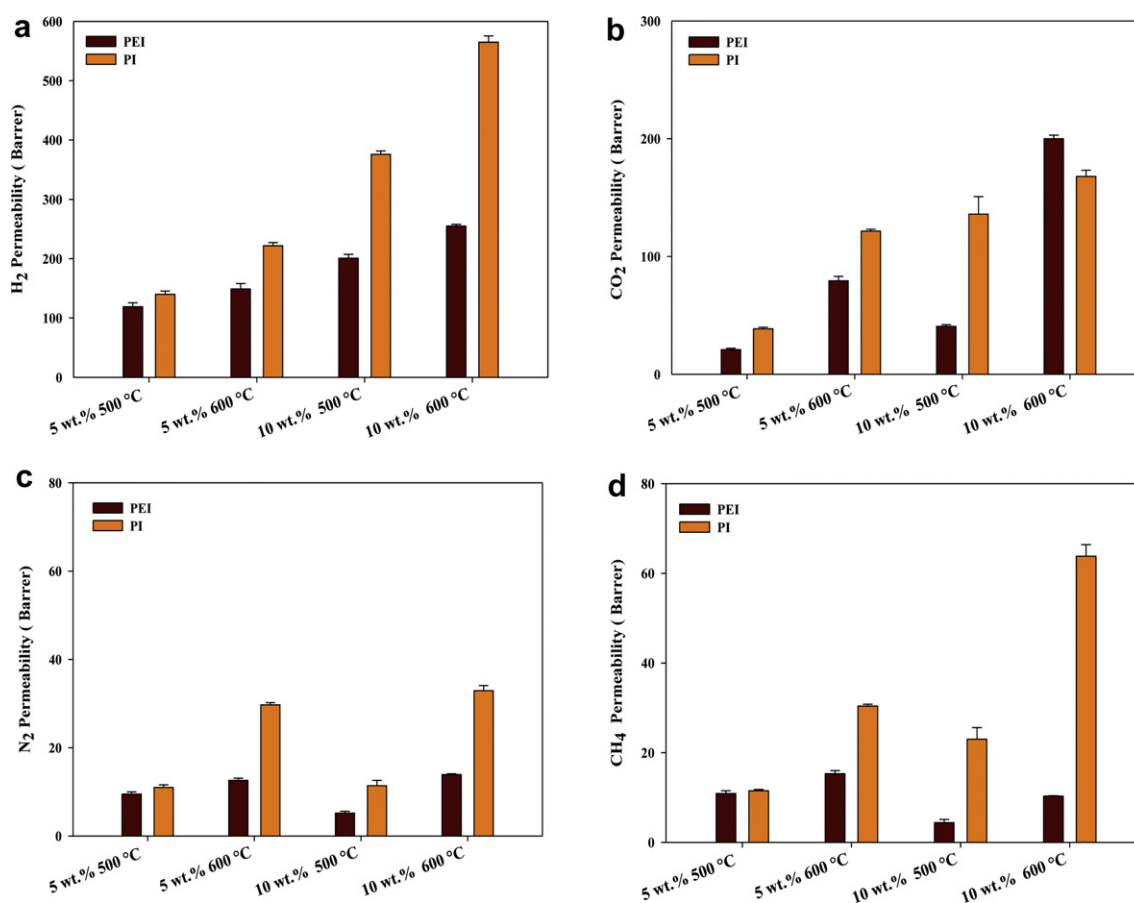

Fig. 7 — Effects of polymer concentration and pyrolysis temperature on (a) H_2, (b) CO_2, (c) N_2, and (d) CH_4 permeabilities of PI- and PEI-derived CMS membranes.
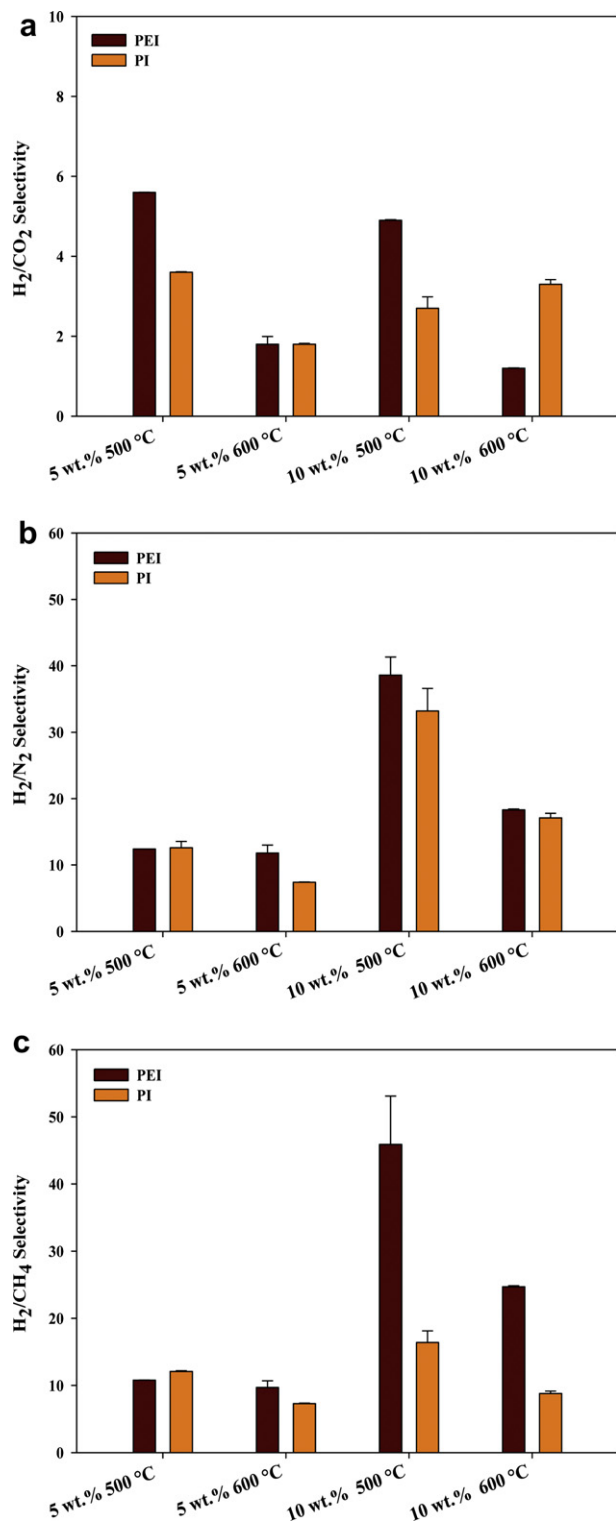
Fig. 8 — Effects of polymer concentration and pyrolysis temperature on (a) H_2/CO_2, (b) H_2/N_2, and (c) H_2/CH_4 permselectivities of PI- and PEI-derived CMS membranes.

phenomenon can also contributed by the high residue carbon in the final carbon matrix.

Comparing with PI-derived CMS membranes, PEI-derived membranes show low permeabilities for H_2, CO_2, N_2 and CH_4. These results consist with the FE-SEM observation that PEI-derived CMS membranes having dense structure even the residue carbon weight were low. This is due to the higher removal rate of volatile solvent or carbon compounds in the PI polymeric matrix at the initial heating stage [28] (as shown in Fig. 2), a partial solvent or carbon vapor may have transpired and created porous structure in the earlier stage (Fig. 5). This would results in high permeability of gases in penetrating through the PI-derived carbon membranes; further, this can also led to decrease the selectivity of H_2/CO_2, H_2/N_2 and H_2/CH_4 gas pair's separation.

For PEI-derived CMS membranes, H_2/CO_2 selectivities of both PEI-5 and PEI-10 membranes pyrolyzed at 500 °C were higher than at 600 °C (Fig. 8a). This may be due to the smaller pore channel created at lower temperature, which suitable for smaller size of gas molecules passed through. Furthermore, PEI-10-500 membranes showed higher permselectivities of H_2/N_2 and H_2/CH_4 gas pairs about 38.6 and 45.9, respectively (Fig. 8b and c). This could be due to C–N stretching and C–C–C bending, whose absorption peaks dominated by the ethers and cyclic ethers groups inhibited the evaporation of the solvent in the membranes at early stages (Fig. 2 and Table 4). Due to the inhibition of solvent evaporation dense texture might have formed on the carbon film when compared with the PI-derived membranes.

Fig. 9 shows the trade-off relationship between (a) H_2 permeability and H_2/N_2 permselectivity, as well as (b) H_2 permeability and H_2/CH_4 permselectivity of PI- and PEI-

similar kind of permeation behavior was observed. The permeability of H_2 and CO_2 were increased with the increasing pyrolysis temperature and concentration of the polymer. However, as the precursor concentration increased to 10 wt.%, the permeability of N_2 and CH_4 slight decreased. This
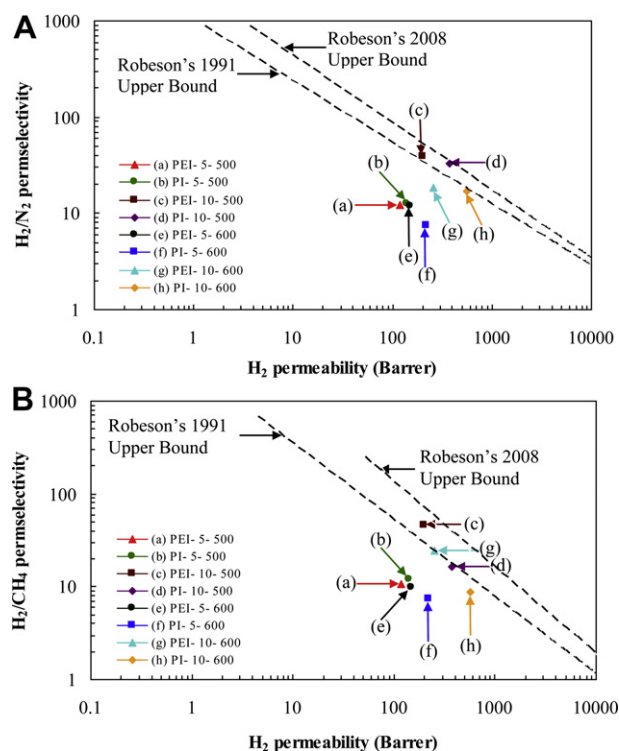
Fig. 9 — Robeson plot for single gas H_2/N_2 and H_2/CH_4 pairs.

Table 5 – Representative H_2, N_2 and CH_4 transport properties of H_2-selective CMS membranes.

Polymeric precursor	Pyrolysis temperature (°C)	Permeation temperature (°C)	Permeability (Barrer)	Selectivity		Reference
			H_2	H_2/N_2	H_2/CH_4	
PPESK[a]	650	30	602	20.3	–	[23]
PEI[b]	600	25	384	2.4	1.7	[36]
PPO[c]	600	25	105	38.9	50.9	[44]
PR[d]	600	35	51.7	28	37	[45]
PFA[e]	600	25	8.1	29.8	–	[46]
PF-resin[f]	800	20	51.2	30.4	29.0	[47]
PI[g]	500	25	376	33.2	16.4	This work
PEI[b]	500	25	201	38.6	45.9	This work

a Poly (phthalazinone ether sulfone ketone) (PPESK).
b Polyetherimide (PEI).
c Polyphenylene oxide (PPO).
d Phenolic resin (PR).
e Polyfurfuryl alcohol (PFA).
f Phenol formaldehyde (PF-resin).
g Polyimide (PI).

derived CMS membranes. As the results indicated that the performances were improved when concentration of the polymer precursor was increased from 5 to 10 wt.% and the pyrolysis temperature was increased from 500 to 600 °C. These results were above the Robeson 1991 upper bound [18] for H_2/N_2 and H_2/CH_4 separation, and close to the Robeson 2008 upper bound curves [19], indicating that the increasing polymer concentration and pyrolysis temperature could enhance gas permeation and separation properties of PI- and PEI-based CMS membranes. The PEI-10-500 exhibited excellent H_2/N_2 and H_2/CH_4 selectivity compared with the other CMS membranes. The results reported in Table 5 represent various CMS membranes prepared and characterized by different investigators for gas separation applications reported in the literature [23,36,44–47]. The present study reported here have superior performance of CMS membranes, when compared with other inorganic membranes in the hydrogen separation.

4. Conclusion

Consideration of functional groups of polymer precursor and pyrolysis condition allows evaluation of the effects of key processing variables for fabrication of CMS membranes. Based on the experimental permeation results and analysis, the following conclusions were made.

1. C=C stretching (in imides) had an intense absorption peak at 1665 cm^{-1}, with PI dominating the insignificant degradation of imide groups at the intermediate stage makes the impact on permeability and as well as permselectivity comparable with PEI-based CMS membranes.
2. For PEI, the adsorption peaks of C=N stretching and C–C–C bending were intense at 1011 and 1068 cm^{-1}, dominated by the ethers and cyclic ethers of asymmetric stretching leads the slightly better permselectivity comparable with the PI-derived CMS membranes
3. For both PI- and PEI-derived CMS membranes the permeability of all gases increased with increasing polymer

concentration, and higher permeability could be obtained for membranes consisted with 10 wt.% and pyrolyzed at 600 °C.
4. The pyrolysis temperature during the pyrolysis process is an important parameter in fabricating CMS membranes. It determines the degree of flexibility of the polymer chain during membrane formation, which in turn influences contact between polymer concentration and pyrolysis temperature.
5. The research results were above the Robeson 1991 upper bound for H_2/N_2 and H_2/CH_4 separation, and very close to the Robeson 2008 upper bound revisited curves, indicating that great potential for hydrogen gas separation *via* microporous alumina support.

Finally, the CMS membranes have great potential for application in hydrogen gas separation.

REFERENCES

[1] Manzolini G, Tosti S. Hydrogen production from ethanol steam reforming: energy efficiency analysis of traditional and membrane processes. Int J Hydrogen Energy 2008;33: 5571–82.
[2] Bilge Y, Mujid SK. Efficiency of hydrogen production systems using alternative nuclear energy technologies. Int J Hydrogen Energy 2006;31:77–92.
[3] Sircar S, Golden TC. Purification of hydrogen by pressure swing adsorption. Sep Sci Technol 2000;35:667–87.
[4] Shao L, Lau CH, Chung TS. A novel strategy for surface modification of polyimide membranes by vapor-phase

ethylenediamine (EDA) for hydrogen purification. Int J Hydrogen Energy 2009;34:8716–22.

[5] Salemme L, Menna L, Simeone M. Analysis of the energy efficiency of innovative ATR-based PEM fuel cell system with hydrogen membrane separation. Int J Hydrogen Energy 2009; 34:6384–92.

[6] Cheng YS, Pena MA, Fierro JL, Hui DCW, Yeung KL. Performance of alumina, zeolite, palladium, Pd–Ag alloy membranes for hydrogen separation from town gas mixture. J Membr Sci 2002;204:329–40.

[7] Shao L, Lowa BT, Chung TS, Greenberg AR. Polymeric membranes for the hydrogen economy: contemporary approaches and prospects for the future. J Membr Sci 2009; 327:18–31.

[8] McCaig MS, Paul DR. Effect of UV crosslinking and physical aging on the gas permeability of thin glassy polyarylate films. Polymer 1999;40:7209–25.

[9] Bos A, Punt IGM, Wessling M, Strathmann H. CO_2-induced plasticization phenomena in glassy polymers. J Membr Sci 1999;155:67–78.

[10] Wach RA, Sugimoto M, Idesaki A, Yoshikawa M. Molecular sieve SiC-based membrane for hydrogen separation produced by radiation curing of preceramic polymers. Mat Sci Eng B 2007;140:81–9.

[11] Shirasaki Y, Tsuneki T, Ota Y, Yasuda I, Tachibana S, Nakajima H, et al. Development of membrane reformer system for highly efficient hydrogen production from natural gas. Int J Hydrogen Energy 2009;34:4482–7.

[12] Lu GQ, Diniz da Costa JC, Duke D, Giessler S, Socolow R, Williams RH, et al. Inorganic membranes for hydrogen production and purification: a critical review and perspective. J Colloid Interface Sci 2007;314(2):589–603.

[13] Lin YS, Kumakiri I, Nair BN, Alsyouri H. Microporous inorganic membranes. Sep Purif Methods 2002;31(2): 229–379.

[14] Saufi SM, Ismail AF. Fabrication of carbon membranes for gas separation-a review. Carbon 2004;42:241–59.

[15] Koros WJ, Mahajan R. Pushing the limits on possibilities for large-scale gas separation: which strategies? J Membr Sci 2000;175:181–96.

[16] Bernardo P, Drioli E, Golemme G. Membrane gas separation: a review/state of the art. Ind Eng Chem Res 2009;48:4638–63.

[17] Grainger S, Hagg MB. Evaluation of cellulose-derived carbon molecular sieve membranes for hydrogen separation from light hydrocarbons. J Membr Sci 2007;306:307–17.

[18] Robeson LY. Correlation of separation factor versus permeability for polymeric membranes. J Membr Sci 1991;62: 165–85.

[19] Robeson LY. The upper bound revisited. J Membr Sci 2008; 320:390–400.

[20] Jung CH, Kim GW, Han SH, Lee YM. Gas separation of pyrolyzed polymeric membranes: effect of polymer precursor and pyrolysis conditions. Macro Mol Res 2007; 15(6):565–74.

[21] Chengwen S, Tonghua W, Huawei J, Xiuyue W, Yiming C, Jieshan Q. Gas separation performance of C/CMS membranes derived from poly (furfuryl alcohol) (PFA) with different chemical structure. J Membr Sci 2010;361:22–7.

[22] Cong H, Radosz M, Towler BF, . Shen Y. Polymer-inorganic nanocomposite membranes for gas separation. Sep Purif Technol 2007;55:281–91.

[23] Zhang B, Wang T, Wu Y, Liu Q, Liu S, Zhang S, et al. Preparation and gas permeation of composite carbon membranes from poly (phthalazinone ether sulfone ketone). Sep Purif Technol 2008;60:259–63.

[24] Wang H, Zhang L, Gavalas GR. Preparation of supported carbon membranes from furfuryl alcohol by vapour deposition polymerization. J Membr Sci 2000;177:25–31.

[25] Song C, Wang T, Wang X, Qiu J, Cao Y. Preparation and gas separation properties of poly (furfuryl alcohol)-based C/CMS composite membranes. Sep Purif Technol 2008;58:412–8.

[26] Hayashi J, Mizuta H, Yamamoto M, Kusakabe K, Morooka S. Pore size control of carbonized BPTA-pp′ ODA polyimide membranes by chemical vapour deposition of carbon. J Membr Sci 1997;124:243–51.

[27] Geiszler VC, Koros WJ. Effects of polyimide pyrolysis conditions on carbon molecular sieve membrane properties. Ind Eng Chem Res 1996;35:2999–3003.

[28] Centeno TA, Vilas JL, Fuertes AB. Effects of phenolic resin pyrolysis conditions on carbon membrane performance for gas separation. J Membr Sci 2004;228:45–54.

[29] Lee HJ, Suda H, Haraya K. Characterization of the post-oxidized carbon membranes derived from poly (2,4-dimenthyl-1,4-phenylene oxide) and their gas permeation properties. Sep Purif Technol 2008;59:190–6.

[30] Zhang X, Hu H, Zhu Y, Zhu S. Effect of carbon molecular sieve on phenol formaldehyde novolac resin based carbon membranes. Sep Purif Technol 2006;52:261–5.

[31] Yoshimune M, Haraya K. Flexible carbon hollow fiber membranes derived from sulfonated poly (phenylene oxide). Sep Purif Technol 2010;75:193–7.

[32] Kim YK, Lee JM, Park HB, Lee YM. The gas separation properties of carbon molecular sieve membranes derived from polyimides having carboxylic acid groups. J Membr Sci 2004;235:139–46.

[33] Mayumi K, Paul JW, William JK. Effect of polymer precursors on carbon molecular sieve structure and separation performance properties. Carbon 2010;48:4432–41.

[34] Lingling Z, Gaohong H, Wei Z, Ming T, Xiangcun L. Effect of formamide additive on the structure and gas permeation performance of polyetherimide membrane. Sep Purif Technol 2010;73:188–93.

[35] Fuertes AB, Centeno TA. Carbon molecular sieve membranes from polyetherimide. Micropor Mesopor Mater 1998;26:23–6.

[36] Itta AK, Tseng HH, Wey MY. Effect of dry/wet-phase inversion method on fabricating polyetherimide-derived CMS membrane for H_2/N_2 separation. Int J Hydrogen Energy 2010;35:1650–8.

[37] Krevelen DW. Properties of polymers. New York: Elsevier Science Publication; 1990.

[38] Takekoshi T. In: Ghosh Malay K, Mittal KL, editors. Polyimides: fundamental and applications. New York: Marcek Dekker; 1996. p. 7.

[39] Loh IH, Oliver W, Sioshansi P. Conducting polymers by ion implantation. Nucl Intsrum Methods Phys Res B 1988;34: 337–46.

[40] Davenas J. Influence of the temperature on the ion beam induced conductivity of polyimide. J Appl Surf Sci 1989;43: 218–23.

[41] Tin PS, Xiao Y, Chung TS. Polyimide-carbonized membranes for gas separation: structural, composition, and morphological control of precursors. Sep Purif Rev 2006;35: 285–318.

[42] Sandeep K, Bin L, Santiago C, Russ GM, Wei-Hong Z. Dramatic property enhancement in polyetherimide using low-cost commercially functionalized multi-walled carbon nanotubes via a facile solution processing method. Nanotechnology 2009;20(465708):1–9.

[43] Rao PS, Wey MY, Tseng HH, Kumar IA, Weng TH. A comparison of carbon/nanotube molecular sieve membranes with polymer blend carbon molecular sieve membranes for the gas separation. Micropor Mesopor Mater 2008;113: 499–510.

[44] Weng TH, Tseng HH, Wey MY. Fabrication and characterization of poly (phenylene oxide)/SBA-15/carbon

molecule sieve multilayer mixed matrix membrane for gas separation. Int J Hydrogen Energy 2010;35:6971–83.

[45] Kita H, Maeda H, Tanaka K, Okamoto K. Carbon molecular sieve membrane prepared from phenolic resin. Chem Lett 1997;2:179–80.

[46] Shiflett MB, Foley HC. Ultrasonic deposition of high selectivity nanoporous carbon membranes. Science 1999;285:1902–5.

[47] Wei W, Qin G, Hu H, You L, Chen G. Preparation of supported carbon molecular sieve membrane from novolac phenol-formaldehyde resin. J Membr Sci 2007;303:80–5.